Static and Dynamic Power System Load Emulation in a Converter-Based Reconfigurable Power Grid Emulator

Jing Wang, *Student Member, IEEE*, Liu Yang, *Student Member, IEEE*, Yiwei Ma, *Student Member, IEEE*, Jingxin Wang, *Member, IEEE*, Leon M. Tolbert, *Fellow, IEEE*, Fei (Fred) Wang, *Fellow, IEEE*, and Kevin Tomsovic, *Fellow, IEEE*

***Abstract*—A hardware testbed platform emulating multiple-area power system scenario dynamics has been established aiming at multiple time-scale real-time emulations. In order to mimic real power flow situations in the utility system, the load emulators have to behave like real ones in both their static and dynamic characteristics. A constant-impedance, constant-current, and constant-power (ZIP) model has been used for static load types, while a three-phase induction motor model has been built to represent dynamic load types. In this paper, ways of modeling ZIP and induction motor loads and the performance of each load emulator are discussed. Comparisons between simulation and experimental results are shown as well for the validation of the emulator behaviors. A real-time composite power load emulator is then demonstrated with desired characteristics and detailed transients for representing a power system PQ bus dynamics.**

***Index Terms*—Dynamic performance, numerical method, power electronics load emulator, power hardware-in-the-loop, real-time application, reconfigurable power grid emulator, regenerative converter, starting up transient, three-phase induction motor load, ZIP load.**

NOMENCLATURE

$V_{\rm dc}$	Three-phase power converter dc voltage value.
$P_{\rm base}, V_{\rm base}, f_{\rm base}$	Three-phase power converter power, voltage, and frequency base for per unit value conversions.
$f_{\rm sw}$	Power converter switching frequency.
V^{pu}, V_d^{pu}, V_q^{pu}	Load bus voltage amplitude, voltage on *d* and *q* axes in per unit.
P^{pu}, Q^{pu}	Real and reactive power of load bus in per unit.
P_0^{pu}, Q_0^{pu}	Real and reactive constant impedance, current and power (ZIP) power base value of load bus in per unit.
p_1, q_1	Coefficients for constant impedance for ZIP real and reactive power.
p_2, q_2	Coefficients for constant current for ZIP real and reactive power.
p_3, q_3	Coefficients for constant power for ZIP real and reactive power.
k_{pf}, k_{qf}	Coefficients for load frequency dependence for ZIP real and reactive power.
P_{ZIP}^{pu}, Q_{ZIP}^{pu}	Real and reactive power of ZIP load in per unit.
$I_{d\_ZIP\_\rm ref}^{pu}$, $I_{q\_ZIP\_\rm ref}^{pu}$	Current references from ZIP model on *d* and *q* axes in per unit.
v_{qs}^{pu}, v_{ds}^{pu}	Three-phase induction motor stator voltage on *q* and *d* axes in per unit.
v_{qr}^{pu}, v_{dr}^{pu}	Three-phase induction motor rotor voltage on *q* and *d* axes in per unit.
i_{qs}^{pu}, i_{ds}^{pu}	Three-phase induction motor stator current on *q* and *d* axes in per unit.
i_{qr}^{pu}, i_{dr}^{pu}	Three-phase induction motor rotor current on *q* and *d* axes in per unit.
r_s^{pu}, r_r^{pu}	Three-phase induction motor stator and rotor leakage resistances in per unit.
ω^{pu}, ω_r^{pu}	Three-phase induction motor stator electrical angular frequency and rotor angular frequency in per unit.
θ	Phase angle of phase A voltage from phase-lock loop (PLL), used for *dq* transformation.
X_M^{pu}	Three-phase induction motor mutual reactance in per unit.
X_{ss}^{pu}, X_{rr}^{pu}	Three-phase induction motor stator and rotor reactance including mutual and leakage reactances in per unit.
T_{em}^{pu}, $T_{\rm load}^{pu}$	Three-phase induction motor electromagnetic and load torque in per unit.
H	Three-phase induction motor inertia constant in per unit.
p	Induction motor pole pairs.

Manuscript received August 22, 2014; revised December 16, 2014 and May 2, 2015; accepted June 8, 2015. Date of publication June 22, 2015; date of current version November 30, 2015. This work was supported primarily by the Engineering Research Center Program of the National Science Foundation and the Department of Energy under NSF Award number EEC-1041877 and the CURENT Industry Partnership Program. Recommended for publication by Associate Editor J. Liu.

The authors are with the Department of Electrical Engineering and Computer Science, The University of Tennessee, Knoxville, Knoxville, TN 37996 USA (e-mail: jwang50@utk.edu; lyang17@utk.edu; yma13@utk.edu; jwang78@utk.edu, tolbert@utk.edu, fred.wang@utk.edu; tomsovic@eecs.utk.edu).

Color versions of one or more of the figures in this paper are available online at http://ieeexplore.ieee.org.

Digital Object Identifier 10.1109/TPEL.2015.2448548

I. INTRODUCTION

POWER electronics are known for their versatile control algorithms and different power stage options. By customization and optimization, converters are built to satisfy different application environments. According to converter topology, control requirements, loading conditions, and switching capabilities of semiconductor devices, the closed-loop controlled behavior bandwidth of three-phase power electronic converters could be designed at several kilohertz [1].

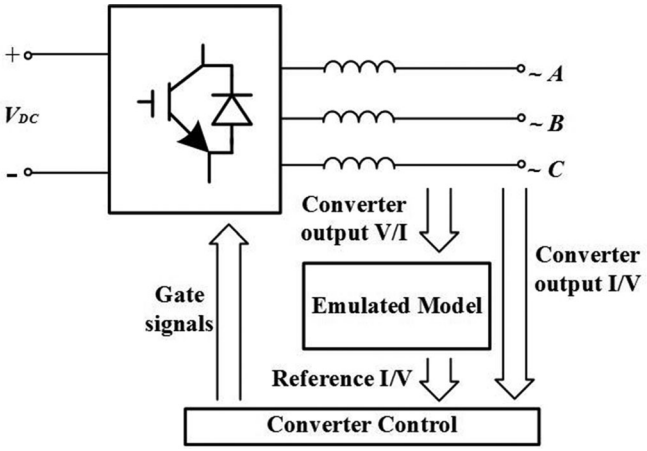

Fig. 1. Three-phase power electronic converter-based emulator unit (Power Hardware-In-The-Loop).

Because of their fast, accurate, and flexible closed-loop behaviors, it is feasible to control power electronic converters to mimic static or slower time electrical dynamics, in order to provide scaled hardware prototypes for algorithm test platform and system behavior estimation [10]–[22]. As illustrated from a three-phase emulator unit example shown in Fig. 1, this converter application is designed to react within its control bandwidth capability to track current/voltage references from the emulated model. The three-phase ac side of the converter is the electrical behavior interface with the rest of the electrical system. Voltage/current inputs are sampled in real time for updating the emulated model calculation. The references from the model will be given to the converter closed-loop controller, so that the electrical behavior from the three-phase interface will represent that of the model.

Previous "Power Hardware-In-The-Loop (PHIL)" (emulator) research, which is based on applications of power electronic converters amplifying digital signal-based models, has been adopted for power system (microgrid, renewables) study [10]–[15] and virtual machine (drive) implementation [19]–[22]. Most commonly, the emulated models are programmed either as a network model or individual object model.

The network models are simulated inside a digital simulator in real-time (usually field-programmable gate array-based simulation tool) to form a network; signals from the simulation are amplified from chosen terminals to interface with the rest of the power hardware of the scenario [10]–[15]. This network simulation-based emulator type can represent large-scale dynamics with minimum hardware resources. However, for the other nodes and buses inside the network, there are no power terminals available because of the simulation-based system scenario characteristics.

For other applications, the emulated object model is implemented inside a digital signal processor (DSP) (or MATLAB/Simulink with dSpace), together with the converter control algorithms and operation. Examples of this type of emulation could be found in [18]–[21], with the majority of the applications being virtual machines. The individual emulator has the advantages of being independently controllable and representable for the actual physical electrical component unit in scenarios.

Combining the advantages of the aforementioned two types of emulators, a reconfigurable power grid emulator-based hardware testbed (HTB), containing both power system network concepts and individual controlled emulators, has been established for real-time grid study and research [16]–[18], [26]–[33]. With appropriate recording techniques, the HTB platform integrates the advantages of both monitoring broader time scale power system model behaviors, and observing detailed performances utilizing the power converters' high tracking bandwidth. Power system components, including the generators, transmission lines, loads, and renewables are emulated by three-phase power electronic converters. By connecting the multiple modular and reconfigurable units together, flexible network and scenario emulation could be demonstrated [27], [29], [32], [33].

Fig. 2(a) shows a typical two-area system with four conventional generators, two load centers, and an interconnecting long-distance transmission line between the two areas [25]. The corresponding real-time emulation network structure consisting of real power electronic converter hardware is shown in Fig. 2(b), with red highlighted three-phase interface as grid emulation dynamics analysis platform.

Following the idea of real-time power emulation, in Fig. 2, G1–4 converters with filtering inductors represent four synchronous generators while L7 and 9 with filtering inductors stand for load centers. The transmission line from bus 7–9 is substituted by the corresponding emulator. The power flow is shown with green arrows: from generator to load and also transmitted from Area 1 to Area 2 (bus 7–9).

The whole structure is reconfigurable by modular power electronics emulators and could be changed to emulate a different power system structure.

The hardware unit photographs for HTB are in Fig. 3. Each single emulator unit contains a three-phase dc/ac converter (based on modified Vacon commercial motor drive), with customized voltage and current sensing and signal conditioning boards. The DSP used in this testbed is TMS320F28335 [40] integrated by Spectrum Digital eZdsp peripherals. As illustrated in Fig. 3(a) and (b), each single cluster includes: active rectifier for establishing and stabilizing dc-bus voltage, generators 1 and 2 in each area, combined static and dynamic load, and local transmission line inductors. Fig. 3(e) shows the whole communication, control and visualization frame of the HTB.

CompactRIO from National Instruments is used to collect information from converter sensing signals by DSP CAN bus [30]. The signals from CompactRIO and Phasor Measurement Unit (PMU) are fed through Ethernet to Labview independent operation centers for status estimation, while commands are delivered through the same network frame backwards in the same communication frame. Control center computer screens are shown on a video wall for real-time update and visualization.

To fulfill this power system testbed function of testing and implementing higher level control methods, such as multiarea

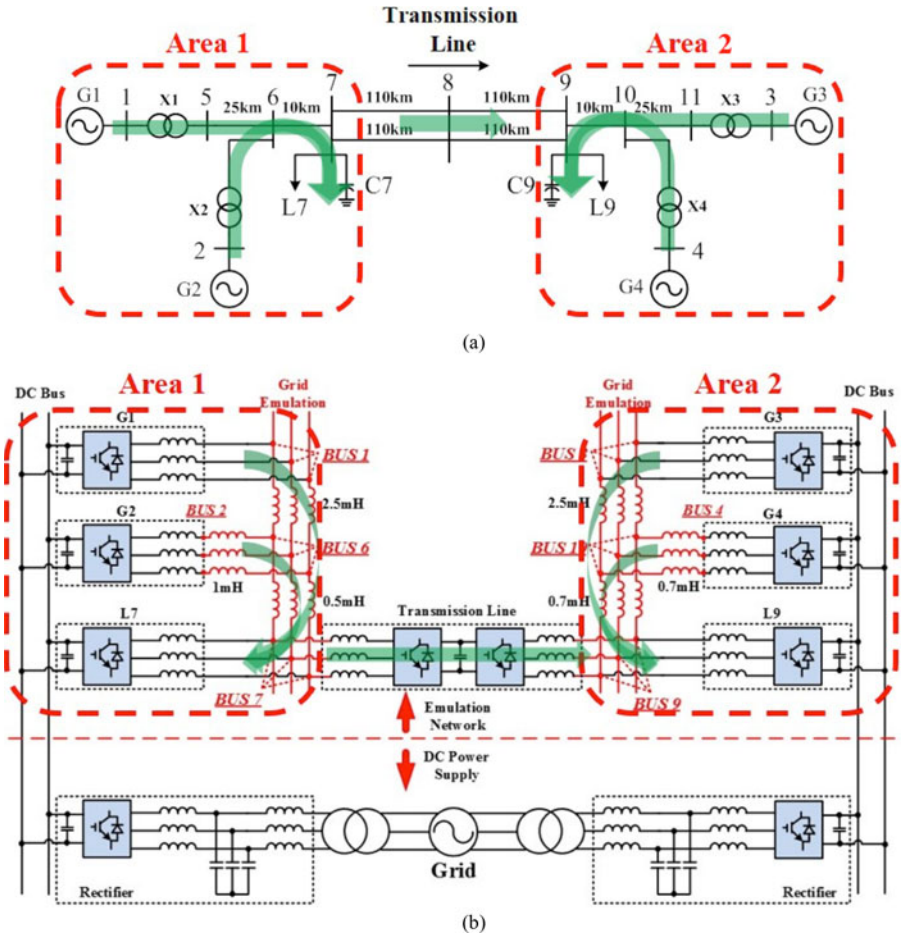

Fig. 2. Example two-area power system: (a) scenario and (b) corresponding configuration of HTB.

automatic generation control algorithms, and real-time monitoring estimation techniques, such as PMU, a comprehensive real-time responsive power load emulator is needed to provide loading conditions for the various power system scenarios. Although it is impossible to define a fixed load model for a universal power distribution system, standard multiple load models for power flow and dynamic simulation programs are recommended in [1], where static and an induction motor model are combined as a composite load model for loading profiles per bus in power system study in the areas of transient stability, long-term dynamics, and small-disturbance stability programs.

In order to provide the HTB real-time emulation platform with flexible power system loading scenarios, detail-rich and accurate PQ load bus model with multiple profiles representing steady state as well as dynamic characteristics has been established and programmed for quantifying the emulators' behaviors.

In this paper, Section II discusses the basic emulator unit topology and some of its features including current controlled type load emulator design and development, in terms of its control structure, dynamic tracking capability, related stability, numerical concerns and real-time implementation time frame. Section III focuses on three-phase static power loading model development, with characteristics of constant impedance, current, and power, with features of variations with voltage and frequency, for representing power system steady-state load conditions. Section IV provides the three-phase dynamic power loading conditions development, representing large industrial motor online starting transients, as well as full details of stator and rotor dynamics. The focus of Section V is the power emulator represented by a PSS/E profiled composite power system load and its experimental performance in real time.

II. Load Emulator Unit

The load emulator was first developed by researchers to substitute for passive loads and provide flexible loading conditions during testing power electronic converter applications such as uninterruptable power supplies, transformers, switching devices, and protection functions. It works as a current sink with various static or dynamic current behaviors [20], [21], [23], [24]. Different from conventional *RLC* load, a power electronic load offers the option of flexibly representing loading conditions desired and circulating the energy, which is especially beneficial for high power applications.

The load emulator functions as a controlled active rectifier mode (see Fig. 4). Three-phase currents are sampled in real time for closed-loop control; three-phase voltages are sampled

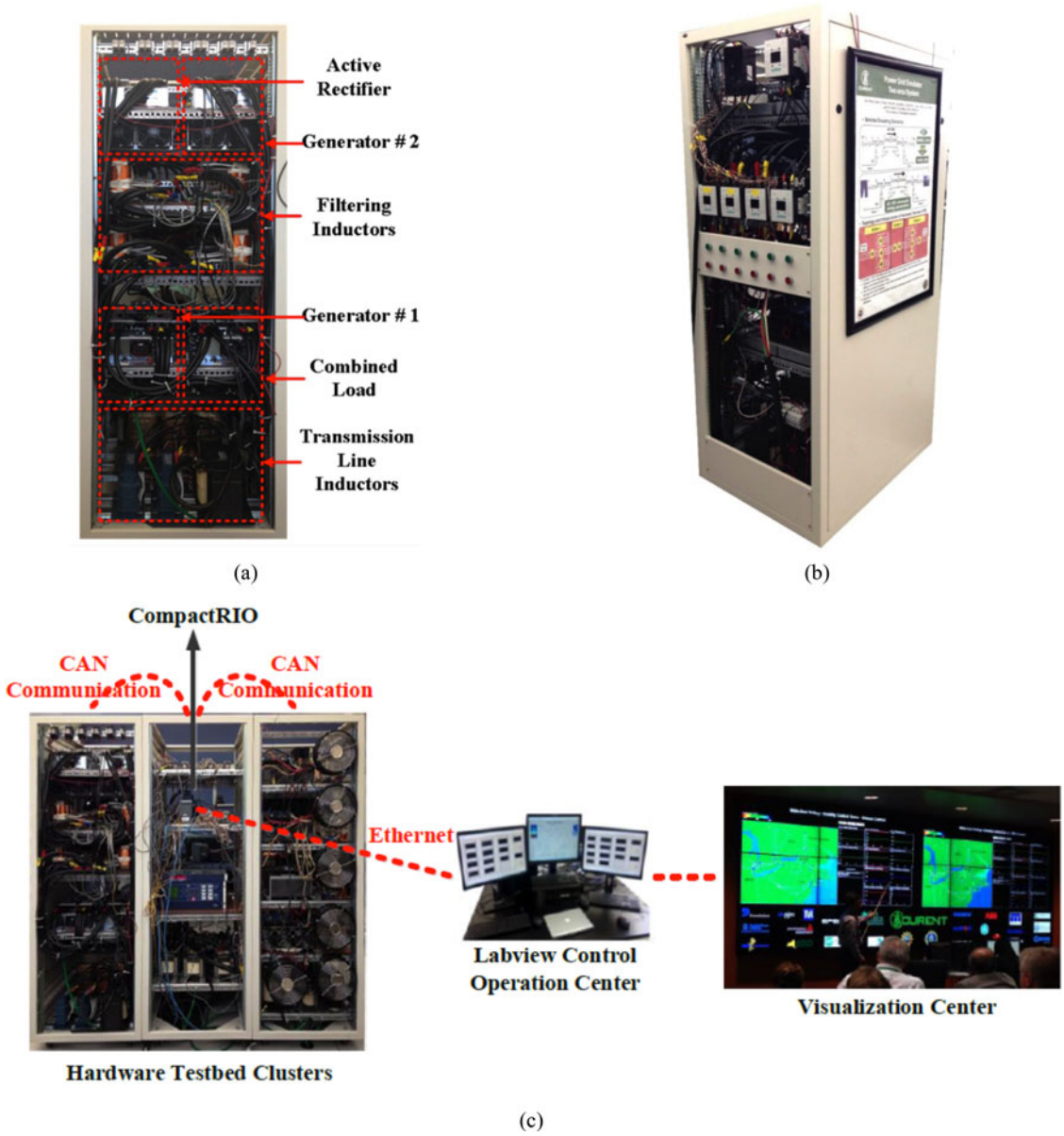

Fig. 3. Experimental hardware of HTB: (a), (b) back and front views of a whole cluster representing a single area, (c) HTB communication and control structure.

and phase locked to frequency and phase angle for power invariant *dq* transformation [25]; and real-time input updates for the emulated model are provided.

For the determination of each emulator unit current controller parameters, classical three-phase *dq* averaging circuit is analyzed for small signal stability around a steady-state operating point [1]. The current control system is a classical PI controller designed in *dq* frame with decoupled *d* and *q* axes. The calculation for each switching interval current reference and actual duty cycle is done within the DSP (details in the D point in this section). In the emulator implementation, the three-phase currents are controlled to behave like the references calculated from the real-time power system load model.

Compared with other general-purpose current controlled power converters, there are several technical challenges for the load emulator developments within the HTB, including the concerns on stability, accuracy and real-time implementation of the composite load emulator.

A. Paralleled Converter Stability and Circulating Current Within a Paralleled Structure

Although multiple converters are connected in a paralleled structure in the HTB, only the three-phase ac interface contains the current and voltage variables that are dynamically closed-loop controlled. Due to the regenerative structure, the dc interface for the system has high equivalent load impedance for the dc voltage regulating rectifier, which is connected to the utility grid and compensates for the whole HTB structure's power loss.

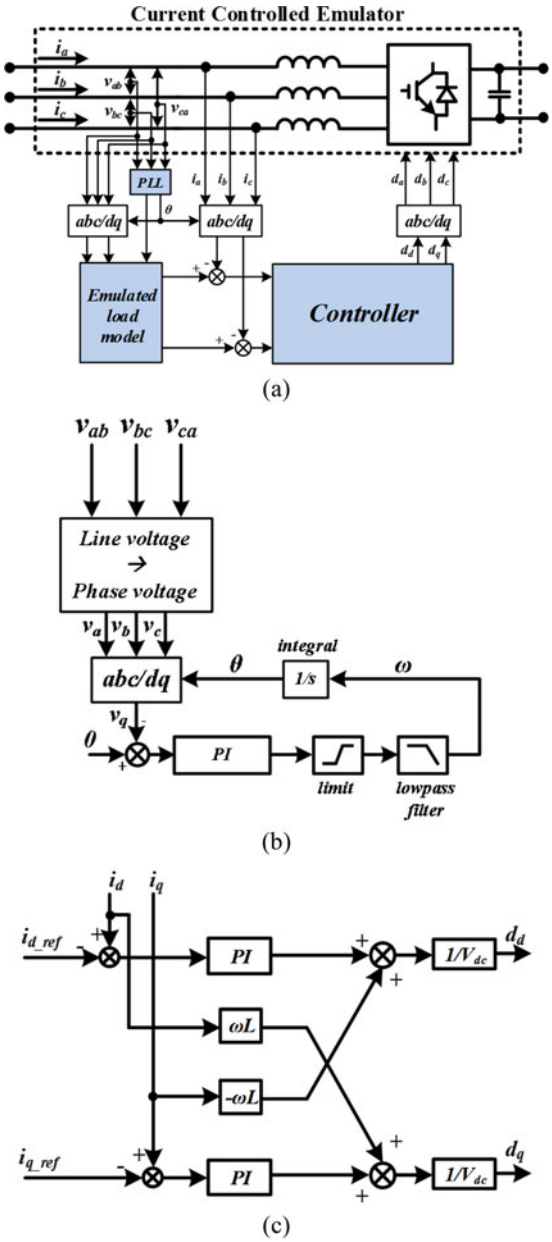

Fig. 4. Load emulator unit implementation: (a) structure of current load emulator, (b) PLL closed-loop control structure details, and (c) PI current controller in *dq* domain.

Previous research has studied stability problems involving multiple regulated power converters, by reducing them to a simpler structure unit consisting of a voltage-controlled converter interfacing a current-controlled converter [3], [4]. The stability evaluations are done through source output impedance and load input impedance in *dq* domain and generalized Nyquist criterion for characteristics loci of the impedance return-ratio matrix [4], [5]. Moreover, considerations about converter related factors, such as PLL [7], digital processor time delay, dead-time compensation, voltage feedforward in the current control loop [8] would provide better accuracy insights for the stability evaluations. The structure related factors, such as number of load emulators paralleled, passive inductor (or even *LCL*) filter [6], inductors representing transmission impedance, are also flexible and open stability topics. In the PHIL case, not only the power converter's characteristics should be included in the stability evaluation, but also the emulated model reference influence on the load impedance should be covered as well (in the grid emulation scenario, the emulated model will mostly affect the low frequency domain impedance).

With the paralleled structure, power is circulated among converters. Various measures have been taken to attenuate the circulating current caused by this parallel structure and switching transients in the HTB [30]: 1) synchronization of PWM signals for different converters has been adopted to reduce the switching frequency circulating current; 2) common-mode choke; 3) zero-sequence current controller; and 4) dead-time compensation has been developed for optimizing the performance of paralleled converters.

B. Power System Load Performance Transients Tracking Capability

As shown from Fig. 5, the left-side bode plot curves show the open-loop transfer functions for the load emulator power converter on *d*-axis without the compensator and with the adjusted compensator, while the right-side bode plot curves show the closed-loop transfer function on *d*-axis with the adjusted compensator. The designed controller decouples *d* and *q* axes, and transfer function on *q*-axis has identical result as that of *d*-axis (both ac and dc sides of the converter are considered constant voltage in design, because ac-side voltage is controlled by the generator emulator and the dc side is controlled by the rectifier).

With consideration of the digital implementation delay and filtering inductor value for the converter, the current controller bandwidth is designed to be 1.2 kHz. The tracking capability of the emulator is represented in the form of a current controlled closed-loop transfer function i_d/i_{dref}. Theoretically, the frequency range covering 0 dB and 0° in the closed-loop transfer function bode figures represents the frequency range for the emulator to track without distortion in amplitude or time delay. The modified emulator could track *dq* reference signals with up to 100 Hz variation within 0.35 dB distortion in amplitude and 4° in phase delay, as measured from Fig. 5.

The target loads for emulation in HTB are power system static and dynamic loads. As concluded in [37], the approximate time scale for power flow (static load) is seconds, sometimes minutes or even longer, which is well within the capable tracking frequency of the emulator. Induction motor load, which contributes to most of the load transients in transmission level grid dynamics, has higher frequency variations.

Fig. 6 illustrates the startup transient for the induction motor model in electric machine synchronous *qd*0 coordinates [34] applied in the test: after frequency-domain analysis, current magnitude corresponding to frequencies higher than 100 Hz is negligible. The overall and detailed figures in Fig. 7 further confirm the experimental tracking performance of the induction motor emulator. The load emulator in this application uses a three-phase full-bridge converter with insulated-gate bipolar

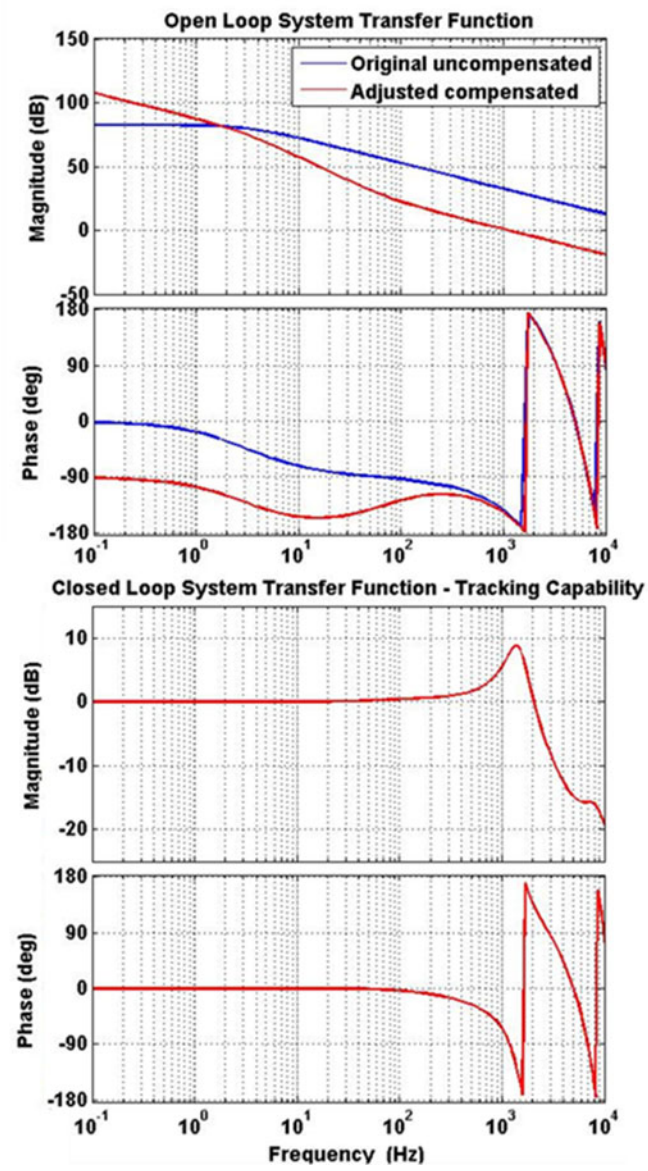

Fig. 5. Controller design and tracking capability of the load emulator.

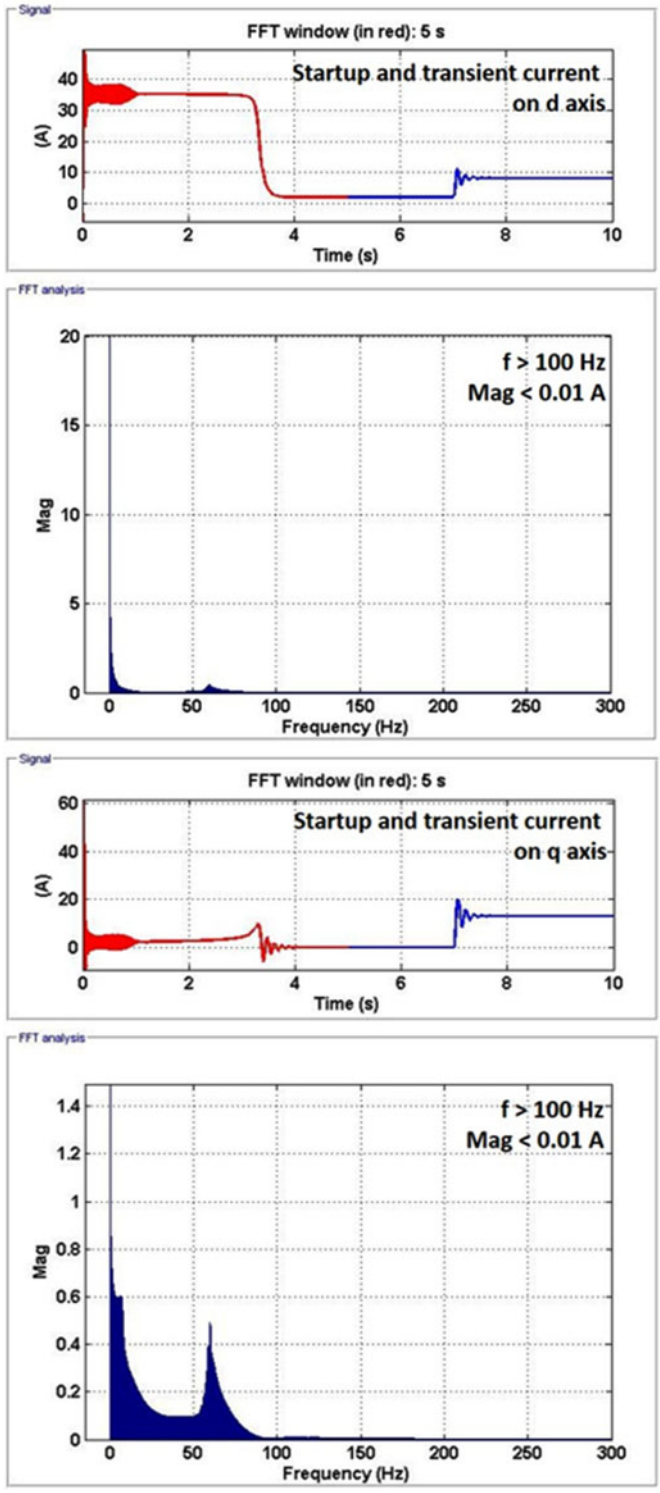

Fig. 6. Frequency analysis of simulated induction motor startup current dynamics.

transistors (IGBTs) switching at 10 kHz, and the designed controller is capable of amplifying the transients represented in the model with minimal distortion.

C. Accuracy of Emulated Load Model

Static [25] and dynamic [34] load model types are established with classical mathematical equations. Further details and non-ideal characteristics of the models will be considered if required by the applications.

Within the limited available computation resource, the current references are calculated in real time. Numerical issues, especially due to the high order of the numerical model, insufficient time step, and improper numerical methods, may result in discrete-time approximation inaccuracies, steady-state errors or delays of the calculation results [38], [39]. Computer simulation tools, such as MATLAB/Simulink, offer higher order discrete approximation and bounded numerical error capability with longer calculation time. Thus, in the later sections, simulation results are used as references to verify load emulator experimental results under the same input conditions.

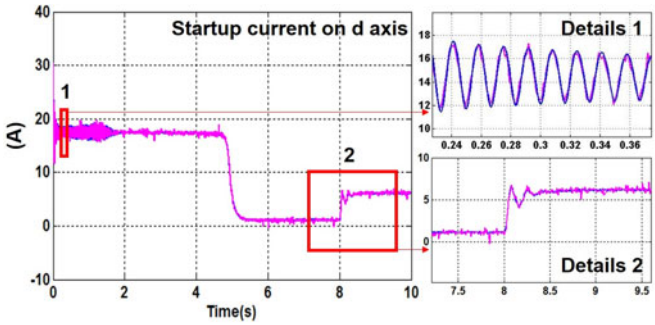

Fig. 7. Detailed example of a recorded experimental results comparing dynamic emulator current references and outputs in *dq*.

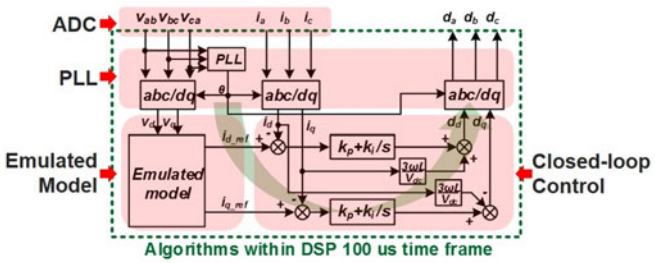

Fig. 8. Real-time algorithms in DSP and implementation timing sequence.

D. Real-Time Implementation Sequence in DSP

The real-time implementations platform in this emulation prototype is digital microprocessor DSP Texas Instruments TMS320F28335 with clock frequency of 150 MHz (6.67 ns cycle time) and 32-bit floating type single precision [39]. All required firmware and software functions are programmed in DSP and running in real time. Fig. 8 illustrates the algorithms within switching cycle of 100 μs time frame inside the digital controller. They include analog digital conversion and signal sampling, PLL and *dq* transformations, real-time emulated model calculation, and closed-loop control functionalities.

In order to operate the emulator in real time, the implementation of all DSP algorithms is required to be finished within the time frame of each time step. Under this application, each function block inside the DSP is optimized, sequenced, and timed as shown in Fig. 9. The emulated model illustrated in the example is a combination of ZIP and two motor models. And the implementation of the motor models depends on the discretization numerical methods applied (example is using fourth-order Runge–Kutta). The CAN communication function is not routinely implemented in each time step—it is irregularly interrupted in the DSP when a message is received.

It is clearly demonstrated that the real-time load emulator including model implementation and converter control functions is well within the calculation capacity of the DSP chosen for this emulation platform.

III. Static Load Emulator

Three-phase static power loading conditions, with characteristics of constant impedance, current, and power, with features

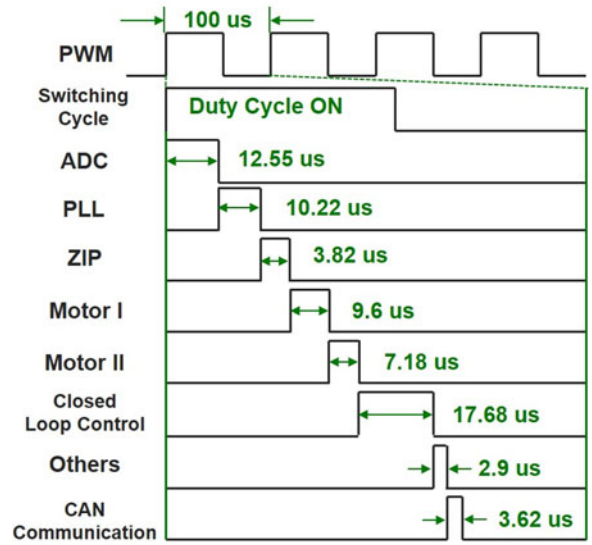

Fig. 9. Timing sequence in DSP and their implementation duration within real-time constraint.

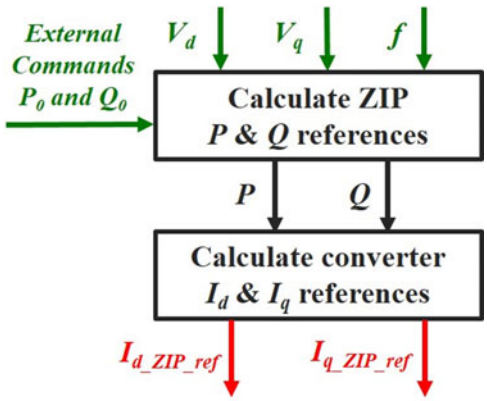

Fig. 10. Real-time ZIP load modeling and implementation in emulator.

of variations with voltage and frequency, and with capability of bidirectional power flow (for representing capacitive power correction devices), are necessary in the development of real-time power system HTB.

Conventional static load model is represented by a series of equations (shown later), which are called ZIP load [1]. They stand for the combination of constant impedance (Z), constant current (I), and constant power (P) loads in both real and reactive power [25].

The real-time implementation and calculation of emulator references are shown in Fig. 10. The emulated ZIP model uses voltages in *dq* domain and emulated grid frequency as inputs for the ZIP model. External base real and reactive power commands are given to the model for specifying the actual power desired by the *PQ* bus power consumption, through Labview manual operations. Outputs desired in the real-time calculation are the current references in *dq* domain to be amplified by the converter.

Commonly adopted in power flow calculations, the ZIP model represents the aggregation of the static characteristics of

TABLE I
ZIP LOAD PARAMETERS AND TEST CONDITIONS

ZIP load model Parameters	Values	Test conditions Parameters	Values
p_1	0.2	$V_{\rm base}$	170 V
p_2	0.2	$P_{\rm base}$	15 kVA
p_3	0.6	$f_{\rm base}$	60 Hz
k_{pf}	1	$V_{\rm dc}$	400 V
q_1	0.2	P_0^{pu}	0.6 p.u.
q_2	0.2	Q_0^{pu}	–0.2 p.u.
q_3	0.6	ZIP load bus	9
k_{qf}	–1	f_{sw}	10 kHz

multiple power system loads. The mathematical polynomials are written as (1) and (2) under presumption of minor fluctuations around nominal grid voltage [25]. Also, frequency dependence effect on the load behavior is considered with the coefficients on real and reactive power

$$\boldsymbol{P}_{\boldsymbol{ZIP}}^{\rm pu} = \boldsymbol{P}_0^{\rm pu} * \left(\boldsymbol{p}_1 \left(\boldsymbol{V}^{\rm pu}\right)^2 + \boldsymbol{p}_2 \left(\boldsymbol{V}^{\rm pu}\right) + \boldsymbol{p}_3\right) * (1 + \boldsymbol{k_{pf}} \Delta f^{\rm pu}) \quad (1)$$

$$\boldsymbol{Q}_{\boldsymbol{ZIP}}^{\rm pu} = \boldsymbol{Q}_0^{\rm pu} * \left(\boldsymbol{q}_1 \left(\boldsymbol{V}^{\rm pu}\right)^2 + \boldsymbol{q}_2 \left(\boldsymbol{V}^{\rm pu}\right) + \boldsymbol{q}_3\right) * (1 + \boldsymbol{k_{qf}} \Delta f^{\rm pu}). \quad (2)$$

ZIP model could be used to fit the power consumption curves for most kinds of power system loads: higher order polynomials are neglected for simplifying the model. In the meantime, the percentage of *Z*, *I*, and *P* for the system load is determined by aggregating different load types and their usage within the grid. By determining the values for p_1, p_2, p_3 and q_1, q_2, q_3, the static load operating state could be specified [31]. During the case when the load model is represented by static load only, the sum of p_1, p_2, and p_3 is unity and the sum of q_1, q_2, and q_3 is unity. The typical value range for k_{pf} is 0–3 and that for k_{qf} is -2 to 0 [25], corresponding to different loading situations.

When the grid voltage falls below a specified value during a fault-caused sag, the polynomials described earlier no longer represent the real power flow condition, because of the relay protection and stall effect of motors in the grid. Switching static load models to constant impedance expressions becomes necessary under that circumstance. p_2, q_2 and p_3, q_3 will be set to zero and p_1, q_1 will be adjusted in order to accommodate the change [25].

Output currents are calculated using (3) and (4) based on the power equivalence relationship in *dq* domain. The voltage V_q is controlled by PLL to be 0, while $V_{\rm d}$ is calculated based on sampled voltage and the angle extracted from PLL

$$\boldsymbol{I}_{\boldsymbol{d\_ZIP\_ref}}^{\rm pu} = \frac{\boldsymbol{V_q^{\rm pu}} \cdot \boldsymbol{P}_{\boldsymbol{ZIP}}^{\rm pu} + \boldsymbol{V_d^{\rm pu}} \cdot \boldsymbol{Q}_{\boldsymbol{ZIP}}^{\rm pu}}{(\boldsymbol{V_d^{\rm pu}})^2 + (\boldsymbol{V_d^{\rm pu}})^2} \quad (3)$$

$$\boldsymbol{I}_{\boldsymbol{q\_ZIP\_ref}}^{\rm pu} = \frac{\boldsymbol{V_d^{\rm pu}} \cdot \boldsymbol{P}_{\boldsymbol{ZIP}}^{\rm pu} - \boldsymbol{V_q^{\rm pu}} \cdot \boldsymbol{Q}_{\boldsymbol{ZIP}}^{\rm pu}}{(\boldsymbol{V_d^{\rm pu}})^2 + (\boldsymbol{V_d^{\rm pu}})^2}. \quad (4)$$

The ZIP emulator dynamics with model parameters in Table I are presented in Fig. 11. The test conditions are all in per unit values: the external commands P_0 and Q_0 are kept constant; the fluctuations on the voltage and frequency of the network are induced by varying the mechanical power input for the generator G3. At $t = 2$ s, the mechanical power input for G3 has a step increase while at $t = 8.5$ and 14 s, the mechanical power input for G3 has a step decrease.

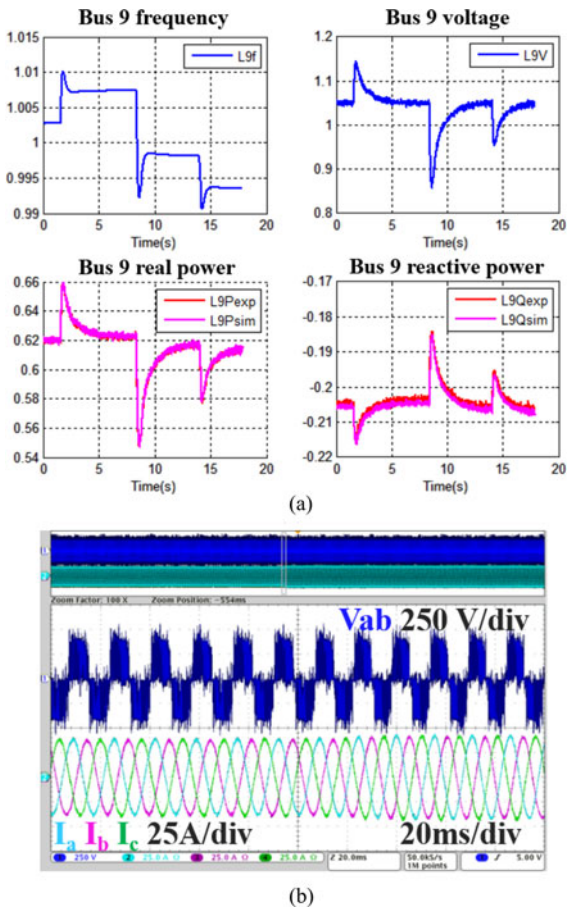

Fig. 11. ZIP emulator (a) P and Q real-time experiment and simulation comparison, (b) experimental waveform.

Fig. 11(a) shows the seconds-scale results obtained from the central visualized operation Labview data recorder, illustrating the power system dynamics slow-changing trend and overall power flow amplitude variations. The close correspondence between simulation and experimental results (bottom left and right) proves the successful emulation of the ZIP load. Fig. 11(b) presents the transients of load increase and decrease in microseconds time scale. Line-to-line voltage is in PWM shape because there is no capacitor filtering in the power circuit. Obvious changes in the current amplitude could be observed, corresponding to the power fluctuations shown in Fig. 11(a).

The emulator experimental waveforms versus simulation results obtained from MATLAB Simulink comparison in Fig. 11(a) illustrates that the output real and reactive power is controlled for the ZIP load emulator, and the emulator responds to the frequency and voltage fluctuations according to expectations.

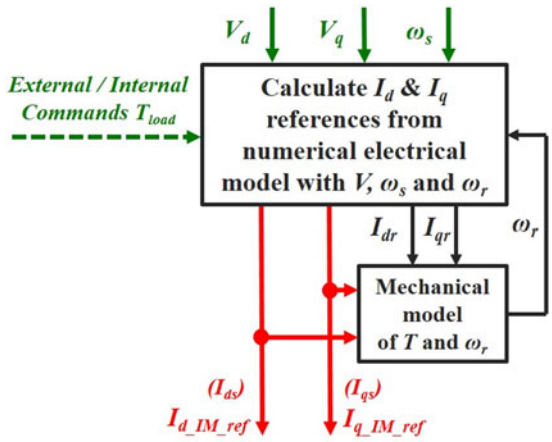

Fig. 12. Real-time induction motor load modeling and implementation in emulator.

IV. Dynamic Load Emulator

Induction motors power most industrial loads, and as such it is the major element contributing to the dynamics and transients for load variations. The high-current start-up process could induce visible grid voltage and frequency fluctuations, while on the other hand, rich dynamic behavior details could be observed under grid variations. An accurate load emulator representing its dynamic behavior is crucial to the system overall loading behavior estimation.

Discrete modeling of an induction motor for real-time signal level calculation of current references is illustrated in Fig. 12. After numerically calculating the current vector containing stator and rotor current variables from the updated input and rotor speed of last time step, the stator current variables are updated as current references for the three-phase power emulator to amplify.

The induction motor per unit model including the electrical and mechanical portions is established in *dq* domain as shown in (5)–(9). Electrical inputs for the model are voltage in *dq* domain and synchronous speed angle from the three-phase voltage. The real-time update of electromagnetic torque and rotor speed in the mechanical model are necessary in calculating accurate current references.

Solving the motor state-space current model represented by time-variant coefficient ordinary differential equations containing vectors of 4×1 variables, the floating point and 32-bit DSP could not provide good calculation accuracy or stability when using simple discrete numerical integration methods. The switching frequency 10 kHz limitation on the IGBT device used in the system causes large time step interval limitation.

Also, the real-time voltage and electrical frequency inputs to the equations will complicate the problem even more.

An upgrade of the numerical method, from first-order explicit Euler (failed in numerical convergence) to third-order accurate Euler-trapezoidal based predictor-corrector method with twice correction PECECE [35], [36] was adopted. Grid-connected direct startup scenario of induction motor emulator is presented in Fig. 13. The parameters for the test scenario is shown in Table II.

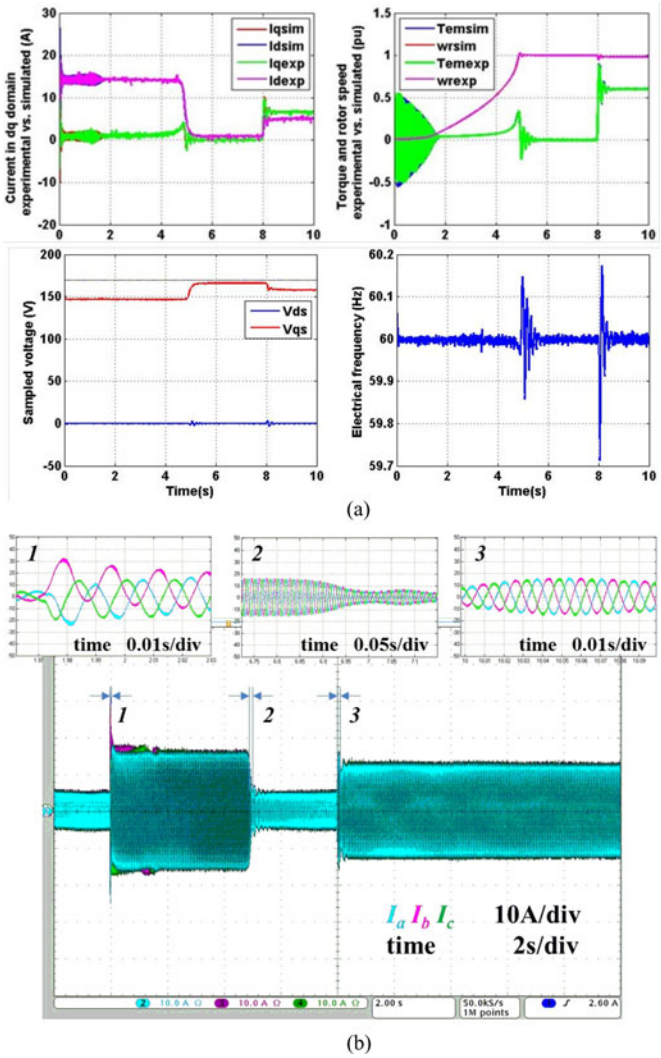

Fig. 13. Induction motor startup process. (a) DSP recorded experimental results in *dq* with simulation. (b) Oscilloscope results overall and detailed shape in *abc*.

TABLE II
Three-Phase Induction Load Model Parameters and Test Conditions

Induction motor load model Parameters	Values	Test conditions Parameters	Values
X_M^{pu}	10.32 p.u.	$V_{\rm base}$	170 V
X_{ss}^{pu}	10.64 p.u.	$P_{\rm base}$	2.55 kVA
X_{rr}^{pu}	10.60 p.u.	$f_{\rm base}$	60 Hz
r_s^{pu}	0.02 p.u.	$V_{\rm dc}$	400 V
r_r^{pu}	0.018 p.u.	Dynamic load bus	9
H	0.13 s	f_{sw}	10 kHz
V_{qr}^{pu} V_{dr}^{pu}	0		
$T_{\rm load}^{pu}$	0 @ 0–8 s 0.6 p.u. @ >8 s		

As shown in Fig. 13(a), the top left part shows the comparison between *dq* currents calculated from simulation and experimental outputs while the top right one shows the comparison between

TABLE III
PERCENTAGE OF COMPOSITE LOAD COMPONENTS IN REAL AND REACTIVE POWER (IN P.U.)

	ZIP		Three-phase large motor 3L			Three-phase small motor 3S		
	Constant power	Constant current	Real power	Capacity	Loading factor	Real power	Capacity	Loading factor
P	33.8%	23.9%	15.7%	15.7%/0.9	0.9	26.6%	26.6%/0.5	0.5
Q	33.8%	23.9%	Q3L			Q3S		

TABLE IV
ZIP AND 3L AND 3S PARAMETERS AND TEST CONDITIONS

ZIP parameters		3L parameters		3S parameters		Test conditions	
Parameter	Value	Parameter	Value	Parameter	Value	Parameters	Values
p_1	0	p_{3L}	2 p.u.	p_{3S}	2 p.u.	$V_{\rm base}$	170 V
p_2	0.239	r^{pu}_{s3L}	0.014 p.u.	r^{pu}_{s3S}	0.037 p.u.	$P_{\rm base}$	15 kVA
p_3	0.338	r^{pu}_{r3L}	0.0117 p.u.	r^{pu}_{r3S}	0.0488 p.u.	$f_{\rm base}$	60 Hz
q_1	0	H_{3L}	1 p.u.	H_{3S}	0.6 p.u.	$V_{\rm dc}$	400 V
q_2	0.239	X^{pu}_{M3L}	3 p.u.	X^{pu}_{M3S}	2.4 p.u.	Load bus	9
q_3	0.338	X^{pu}_{ss3L}	3.08 p.u.	X^{pu}_{ss3S}	2.7626 p.u.	f_{sw}	10 kHz
k_{pf}	0	X^{pu}_{rr3L}	3.11 p.u.	X^{pu}_{rr3S}	2.532 p.u.		
$k_{\rm qf}$	0	$T^{pu}_{\rm Load-3L}$	$0.9*(\omega_{r-3L^{pu}})^2$	$T^{pu}_{\rm Load-3S}$	$0.5*(\omega_{r-3S^{pu}})^2$		

simulation results and calculated T^{pu}_{em} and ω^{pu}_r recorded in the DSP memory. The bottom left and right waveforms present the voltage and frequency inputs (in real value) for the induction motor model during the experiment. The load for the induction motor is a constant torque load: $T^{pu}_{\rm load} = 0$ for $t < 8$ s, and a transient happens at $t = 8$ s, where the $T^{pu}_{\rm load}$ has a step change to 0.6 p.u.

Induction motor emulator startup current waveforms in *abc* domain are observed from Fig. 13(b), with the transients zoom-in pictures on the top of the oscilloscope watch window showing multiple time-scale observations of the emulator behavior: for $t < 2$ s, the emulator reaches steady state, behaving as constant current load of 5 A, while for $t > 2$ s, the induction motor model starts acceleration and changes loading conditions: see equation (5) shown as the bottom of the page

$$\boldsymbol{\lambda^{pu}_{ds}} = \boldsymbol{X^{pu}_{ss}\, i^{pu}_{ds}} + \boldsymbol{X^{pu}_{m}\, i^{pu}_{dr}} \tag{6}$$

$$\boldsymbol{\lambda^{pu}_{qs}} = \boldsymbol{X^{pu}_{ss}\, i^{pu}_{qs}} + \boldsymbol{X^{pu}_{m}\, i^{pu}_{qr}} \tag{7}$$

$$\boldsymbol{T^{pu}_{em}} = \boldsymbol{\lambda^{pu}_{ds}\, i^{pu}_{qs}} - \boldsymbol{\lambda^{pu}_{qs}\, i^{pu}_{ds}} \tag{8}$$

$$\boldsymbol{\omega^{pu}_{r}} = \int_0^t \frac{\boldsymbol{T^{pu}_{em}} - \boldsymbol{T^{pu}_{Load}}}{2\boldsymbol{H}}\boldsymbol{d\tau}. \tag{9}$$

The real-time calculated results exhibit high accuracy and robustness after repetitive tests of the whole startup process and the sudden jump of constant torque load. Less than 2% of difference between simulation (from MATLAB) and experimental results (of emulator) are observed from the *dq* current comparison shown in Fig. 13(a). The stable and robust model references calculation and tracking performances in *dq* and *abc* domains of the load emulator are illustrated in Fig. 13 with the smooth transients and close alignment between the references and the experimental outputs.

V. COMPOSITE POWER SYSTEM LOAD EMULATOR

According to Western Electricity Coordinating Council power system load modeling approach, static and dynamic models are major components mapping to different end-use load

$$\begin{bmatrix} v^{\rm pu}_{qs} \\ v^{\rm pu}_{ds} \\ v^{\rm pu}_{qr} \\ v^{\rm pu}_{dr} \end{bmatrix} = \begin{bmatrix} r^{\rm pu}_s & \omega^{\rm pu}\cdot X^{\rm pu}_{ss} & 0 & \omega^{\rm pu}\cdot X^{\rm pu}_M \\ -\omega^{\rm pu}\cdot X^{\rm pu}_{ss} & r^{\rm pu}_s & -\omega^{\rm pu}\cdot X^{\rm pu}_M & 0 \\ 0 & (\omega^{\rm pu}-\omega^{\rm pu}_r)\cdot X^{\rm pu}_M & r^{\rm pu}_r & (\omega^{\rm pu}-\omega^{\rm pu}_r)\cdot X^{\rm pu}_{rr} \\ -(\omega^{\rm pu}-\omega^{\rm pu}_r)\cdot X^{\rm pu}_M & 0 & -(\omega^{\rm pu}-\omega^{\rm pu}_r)\cdot X^{\rm pu}_{rr} & r^{\rm pu}_r \end{bmatrix} \cdot \begin{bmatrix} i^{\rm pu}_{qs} \\ i^{\rm pu}_{ds} \\ i^{\rm pu}_{qr} \\ i^{\rm pu}_{dr} \end{bmatrix} + \begin{bmatrix} X^{\rm pu}_{ss} & 0 & X^{\rm pu}_M & 0 \\ 0 & X^{\rm pu}_{ss} & 0 & X^{\rm pu}_M \\ X^{\rm pu}_M & 0 & X^{\rm pu}_{rr} & 0 \\ 0 & X^{\rm pu}_M & 0 & X^{\rm pu}_{rr} \end{bmatrix} \cdot \frac{1}{\omega_b}\cdot\frac{d}{dt} \begin{bmatrix} i^{\rm pu}_{qs} \\ i^{\rm pu}_{ds} \\ i^{\rm pu}_{qr} \\ i^{\rm pu}_{dr} \end{bmatrix} \tag{5}$$

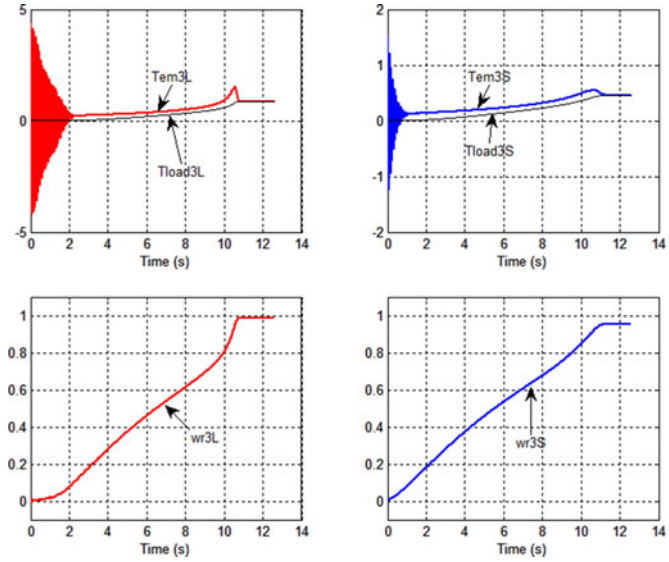

Fig. 14. Experimental 3L and 3S startup DSP record.

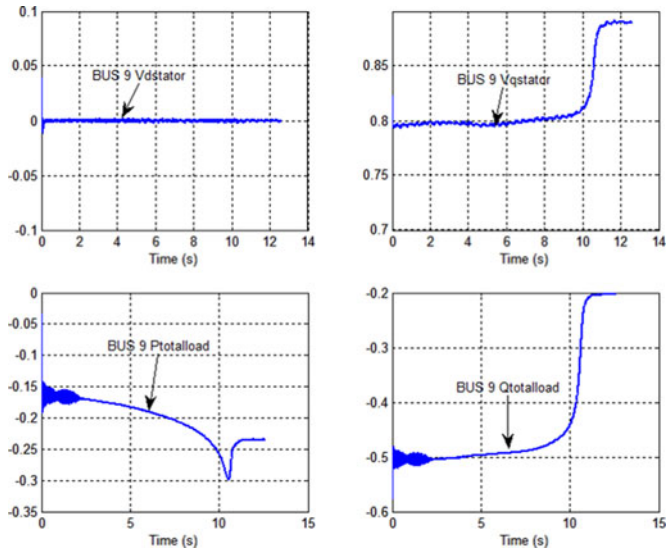

Fig. 15. Experimental bus L9 V and P Q DSP record.

consumptions [31]. The system composite load model could reflect the seasonal change and area substation load class (agricultural, commercial, industrial or residential) by adjusting the percentages within static and dynamic load models [31].

This test scenario is designed to observe the dynamic details in real time for the start-up of a PQ load bus. A composite load model has been developed, consisting of a ZIP static load model, a three-phase large motor (3L), and a three-phase small motor (3S) loading at Bus 9 of the grid schematic configuration shown in Fig. 2. The composite load is intended to represent the dynamic and static load performance using a single load emulator converter.

The compositions of the load model is indicated in Tables III and IV. The ZIP load is modeled to behave as constant power

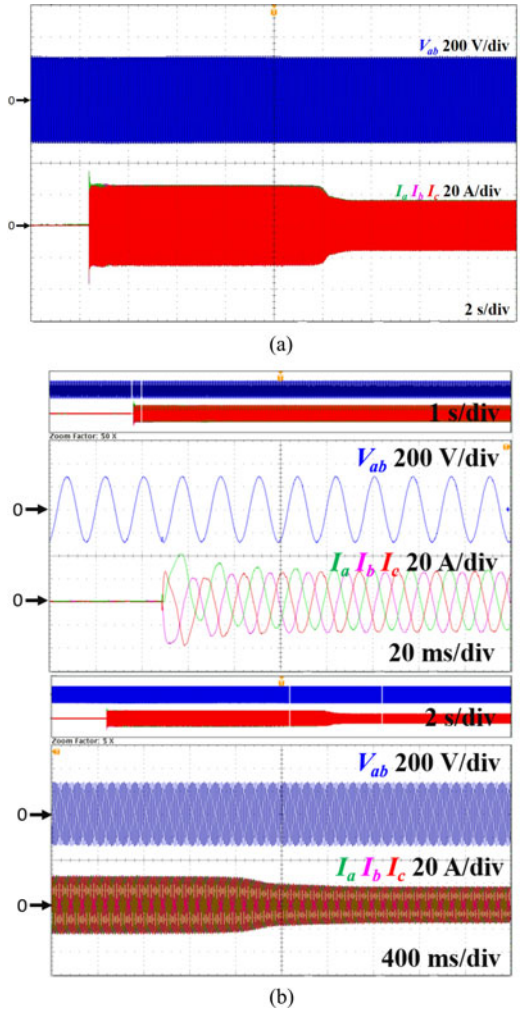

Fig. 16. Details of L9 bus voltage and current waveform for composite power load in *abc* domain.

and current load, while the motor 3L is assumed to be loaded with 0.9 p.u. speed-square-related torque in steady state and motor 3S with 0.5 p.u. speed-square-related torque in steady state (fan or pump type of load). The model parameters are based on PSS/E simulation profile.

In the test configuration shown in Fig. 2, area 2 consists of generator emulator G3, inductor of 3.2 mH representing transformer as well as the local transmission line impedance, and composite load emulator L9 representing combination of static, 3L, and 3S loads. As indicated in Fig. 3, all single area elements installed within a cluster and real-time observation and control platform connected through DSP CAN bus and NI Labview products with bidirectional information exchange.

The recorded real-time experimental variables of motor T_{em}^{pu}, ω_r^{pu}, as well as v_{qs}^{pu}, v_{ds}^{pu}, and load bus P^{pu}, Q^{pu} transients in the DSP memory are shown in Figs. 14 and 15. For each one of the variables, a total length of 12.6 s is recorded, with data resolution of 24 ms.

The induction motors started with a fan/pump type load until reaching steady state. As could be observed from Fig. 15, the

L9 terminal voltage has a period from 0 to 11 s of voltage sag, down to 0.8 p.u., due to motors starting up. While during the same time, the real and reactive powers on L9 bus have similar transients due to the same reason of motor starting. The increase on the real power consumption on L9 is contributed to by the acceleration of the rotor with mechanical load. Reactive power on L9 returns back to a steady-state value close to the ZIP value after the motor establishes the magnetic field during the starting up transient. Similar to the waveform shown in *dq* domain, the waveform shown in Fig. 16 illustrates the composite load behavior in *abc* domain.

VI. Conclusion

This paper focuses on developing a load emulator with power electronic converters. By flexibly programming the load emulator's models in the digital controller, different types of load behaviors are presented.

By combining a ZIP model and multiple induction motor models, a composite load emulator has been developed to represent a PQ bus for power system steady state and transient scenarios. The emulator development in the power system emulation of the HTB enables customizing test power system scenarios for higher level interarea control algorithms testing, as well as real-time monitoring and estimation of the dynamics in multitime scales.

References

[1] IEEE Task Force on Load Representation for Dynamic Performance, "Standard load models for power flow and dynamic performance simulation," *IEEE Trans. Power Syst.*, vol. 10, no. 3, pp 1302–1313, Aug. 1995.

[2] S. Hiti, D. Boroyevich, and C. Cuadros, "Small-signal modeling and control of three-phase PWM converters," in *Proc. Conf. Rec. IEEE Ind. Appl. Soc. Annu. Meeting*, Oct. 1994, pp. 1143–1150.

[3] B. Wen, D. Boroyevich, P. Mattavelli, Z. Shen, and R. Burgos, "Experimental verification of the generalized Nyquist stability criterion for balanced three-phase ac systems in the presence of constant power loads," in *Proc. IEEE Energy Convers. Congr. Expo.*, Sep. 2012, pp. 3926–3933.

[4] R. Burgos, D. Boroyevich, F. Wang, K. Karimi, and G. Francis, "On the ac stability of high power factor three-phase rectifiers," in *Proc. IEEE Energy Convers. Congr. Expo.*, Sep. 2010, pp. 2047–2054.

[5] M. Belkhayat, *Stability criteria for AC power systems with regulated loads*, Ph.D. dissertation, School Electr. Comp. Eng., Purdue Univ., Dec. 1997.

[6] S. Lentijo, S. D'Arco, and A. Monti, "Comparing the dynamic performances of power hardware-in-the-loop interfaces," *IEEE Trans. Ind. Electron.*, vol. 57, no. 4, pp. 1195–1207, Apr. 2010.

[7] B. Wen, D. Boroyevich, P. Mattavelli, Z. Shen, and R. Burgos, "Influence of phase-locked loop on input admittance of three-phase voltage-source converters," in *Proc. IEEE Appl. Power Electron. Conf. Expo.*, Mar. 2013, pp. 897–904.

[8] X. Zhang, F. Wang, W. Cao, and Y. Ma, "Influence of voltage feed-forward control on small-signal stability of grid-tied inverters," in *Proc. IEEE Appl. Power Electron. Conf. Expo.*, Mar. 2015, pp. 1216–1221.

[9] C. M. Wildrick, F. C. Lee, B. H. Cho, and B. Choi, "A method of defining the load impedance specification for a stable distributed power system," *IEEE Trans. Power Electron.*, vol. 10, no. 3, pp. 280–285, May 1995.

[10] M. Steurer, C. S. Edrington, M. Sloderbeck, W. Ren, and J. Langston, "A megawatt-scale power hardware-in-the-loop simulation setup for motor drives," *IEEE Trans. Ind. Electron.*, vol. 57, no. 4, pp. 1254–1260, Apr. 2010.

[11] V. Karapanos, S. de Haan, and K. Zwetsloot, "Real time simulation of a power system with VSG hardware in the loop," in *Proc. IEEE Ind. Electron. Soc. Conf.*, Australia, Nov. 2011, pp. 3748–3754.

[12] P. Kotsampopoulos, A. Kapetanaki, G. Messinis, V. Kleftakis, and N. Hatziargyriou, "A PHIL facility for microgrids," *Int. J. Distrib. Energy Resources*, vol. 9, no. 1, pp. 71–86, Mar. 2013.

[13] W. Zhu, S. Pekarek, J. Jatskevich, O. Wasynczuk, and D. Delisle, "A model-in-the-loop interface to emulate source dynamics in a zonal dc distribution system," *IEEE Trans. Power Electron.*, vol. 20, no. 2, pp. 438–445, Mar. 2005.

[14] A. Emadi and M. Ehsani, "Multi-converter power electronic systems: Definition and applications," in *Proc. IEEE 32nd Power Electron. Spec. Conf.*, Jun. 2001, pp. 1230–1236.

[15] W. Ren, "Accuracy evaluation of power hardware-in-the-loop simulation," Ph.D. dissertation, Dept. Elect. Comput. Eng., Florida State Univ., Tallahassee, FL, USA, 2007.

[16] J. Wang, L. Yang, Y. Ma, X. Shi, X. Zhang, L. Hang, K. Lin, L. M. Tolbert, F. Wang, and K. Tomsovic, "Regenerative power converters representation of grid control and actuation emulator," in *Proc. IEEE Energy Convers. Congr. Expo.*, Sep. 2012, pp. 2460–2465.

[17] J. Wang, L. Yang, Y. Ma, J. Wang, L. M. Tolbert, F. Wang, and K. Tomsovic, "Static and dynamic power system load emulation in converter-based reconfigurable power grid emulator," in *Proc. IEEE Energy Convers. Congr. Expo.*, Sep. 2014, pp. 4008–4015.

[18] J. Wang, Y. Ma, L. Yang, L. M. Tolbert, and F. Wang, "Power converter-based three-phase induction motor load emulator," in *Proc. IEEE Appl. Power Electron. Conf. Expo.*, Mar. 2013, pp. 3270–3274.

[19] M. Armstrong, D. J. Atkinson, A. G. Jack, and S. Turner, "Power system emulation using a real time, 145 kW, virtual power system," in *Proc. Eur. Conf. Power Electron. Appl.*, 2005, pp. 1–10.

[20] Y. S. Rao and M. C. Chandorkar, "Real-time electrical load emulator using optimal feedback control technique," *IEEE Trans. Ind. Electron.*, vol. 57, no. 4, pp. 1217–1225, Apr. 2010.

[21] H. Slater, D. Atkinson, and A. Jack, "Real-time emulation for power equipment development. Part II: The virtual machine," *Proc. Inst. Elect. Eng.*, vol. 145, no. 3, pp. 153–158, May 1998.

[22] T. Boller and R. M. Kennel, "Virtual machine—A hardware in the loop test for drive inverters," in *Proc. 13th Eur. Conf. Power Electron. Appl.*, Sept. 8–10, 2009, pp. 1–5.

[23] S. Gupta and V. Rangaswamy, "Load bank elimination for UPS testing," in *Proc. Conf. Rec. IEEE-IAS Annu. Meeting*, 1990, pp. 1040–1043.

[24] M. Tsai, "Comparative investigation of the energy recycler for power electronics burn-in test," *Proc. Inst. Elect. Eng. Elect. Power Appl.*, vol. 147, no. 3, pp. 92–198, May 2000.

[25] P. Kundur, *Power System Stability and Control*. New York, NY, USA: McGraw-Hill, 1994.

[26] L. Yang, X. Zhang, Y. Ma, J. Wang, L. Hang, K. Lin, L. M. Tolbert, F. Wang, and K. Tomsovic, "Hardware implementation and control design of generator emulator in multi-converter system," in *Proc. IEEE Appl. Power Electron. Conf. Expo.*, Mar. 2013, pp. 2316–2323.

[27] Y. Ma, L. Yang, J. Wang, F. Wang, and L. M. Tolbert, "Emulating full-converter wind turbine by a single converter in a multiple converter based emulation system," in *Proc. IEEE Appl. Power Electron. Conf. Expo.*, Mar. 2013, pp. 3042–3047.

[28] W. Cao, Y. Ma, J. Wang, L. Yang, J. Wang, F. Wang, and L. M. Tolbert, "Two-stage PV inverter system emulator in converter based power grid emulation system," in *Proc. IEEE Energy Convers. Congr. Expo.*, Sep. 2013, pp. 4518–4525.

[29] W. Cao, Y. Ma, J. Wang, and F. Wang, "Virtual series impedance emulation control for remote PV or wind farms," in *Proc. IEEE Appl. Power Electron. Conf. Expo.*, Mar. 2014, pp. 411–418.

[30] Y. Ma, L. Yang, J. Wang, X. Shi, F. Wang, and L. M. Tolbert, "Circulating current control and reduction in a paralleled converter test-bed system," in *Proc. IEEE Energy Convers. Congr. Expo.*, Sep. 2013, pp. 5426–5432.

[31] D. N. Kosterev and A. Meklin, "Load modeling in WECC," in *Proc. IEEE PES Power Syst. Conf. Expo.*, Oct. 2006, pp. 576–581.

[32] L. Yang, J. Wang, Y. Ma, J. Wang, X. Zhang, W. Cao, L. Hang, L. M. Tolbert, F. Wang, and K. Tomsovic, "Development of converter based reconfigurable power grid emulator," in *Proc. IEEE Energy Convers. Congr. Expo.*, Sep. 2014, pp. 3990–3997.

[33] J. Wang, L. Yang, C. Blalock, and L. M. Tolbert, "Flywheel energy storage emulation using reconfigurable hardware test-bed of power converters," in *Proc. Elect. Energy Storage Appl. Technol.*, Oct. 2013.

[34] R. Krishnan, *Electric Motor Drives: Modeling, Analysis, and Control*. Englewood Cliffs, NJ, USA: Prentice-Hall, 2001.

[35] A. Iserles, *A First Course in the Numerical Analysis of Differential Equations*. New York, NY, USA: Cambridge Univ. Press, 2009.
[36] H. E. Jordan, "Digital computer analysis of induction machines in dynamic systems," *IEEE Trans. Power App. Syst.*, vol. PAS-86, no. 6, pp. 722–728, Jun. 1967.
[37] G. Anderson, *Modeling and Analysis of Electrical Power Systems*. Lecture 227–0528–00, Zurich, Switzerland: EEH-Power Systems Laboratory, ETH, 2004, Lecture 227-0528-00, pp. 80–81.
[38] N. S. Gehlot and P. J. Alsina, "A discrete model of induction motors for real-time control applications," *IEEE Trans. Ind. Electron.*, vol. 40, no. 3, pp. 317–325, Jun. 1993.
[39] B. M. Joshi and M. C. Chandorkar, "Time discretization issues in induction machine model solving for real-time applications," in *Proc. IEEE Int. Electr. Mach. Drives Conf.*, May 2011, pp. 675–680.
[40] Texas Instruments. (2015, May). *TMS320F28335* [Online]. Available: http://www.ti.com/product/tms320f28335

Jing Wang (S'09) received the B.S. degree in electrical engineering from the Huazhong University of Science and Technology, Wuhan, China, in 2009, and the M.S. degree in electrical engineering from the University of Tennessee at Knoxville, TN, USA, in 2011, where she received the Ph.D. degree in power electronics, electrical engineering from CURENT in 2015, under the supervision of Dr. Leon M. Tolbert.

Her research interests include three-phase power electronics converter control design, induction motor modeling and emulation, numerical analysis for real-time applications and high efficiency power supplies.

Liu Yang (S'11) received the B.S. and M.S. degrees in electrical engineering from Wuhan University, Wuhan, China, in 2008 and 2010, respectively. She is currently working toward the Ph.D. at the University of Tennessee, Knoxville, USA.

Her research interests include power hardware-in-the-loop, synchronous generator emulation, microgrid, converter control and stability analysis.

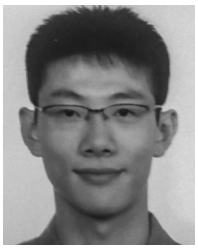

Yiwei Ma (S'13) received the B.S. and M.S. degrees in electrical engineering from Tsinghua University, Beijing, China, in 2009 and 2011, respectively. He is currently working toward the Ph.D. at the University of Tennessee, Knoxville, TN, USA.

His research interests include modeling and control of power electronics interfacing converters for the renewable energy sources, multilevel converters, and microgrids.

Jingxin Wang (S'13–M'15) received the B.S. and M.S. degrees from the China University of Mining and Technology, Jiangsu, China, and the Ph.D. degree from Shanghai Jiaotong University, in 2003, 2006, and 2011, respectively, all in electrical engineering.

He is currently a Research Associate at the University of Tennessee, Knoxville, USA. His research interests include high performance motor control, three-phase converter design, power flow control, and renewable energy.

Leon M. Tolbert (S'88–M'91–SM'98–F'13) received the B.E.E., M.S., and Ph.D. degrees in electrical engineering from Georgia Tech, Atlanta, GA, USA, in 1989, 1991, and 1999, respectively.

He joined Oak Ridge National Laboratory (ORNL) in 1991 and worked on several electrical distribution projects at the three U.S. Department of Energy plants in Oak Ridge, TN, from 1991 to 1999. He joined the University of Tennessee in 1999 and is currently the Min H. Kao Professor and Department Head in Electrical Engineering and Computer Science. He is also a Part-Time Senior Research Engineer at ORNL and conducts joint research in the Power Electronics and Electric Machinery Research Center. He does research in the areas of electric power conversion for renewable energy sources, multilevel converters, utility application of power electronics, microgrids, electric vehicles, and application of wide bandgap (SiC and GaN) power electronics.

Dr. Tolbert is a registered Professional Engineer in the state of Tennessee. He was elected as a member-at-large to the IEEE Power Electronics Society Advisory Committee for 2010–2012, and has served as the Chair of the PELS Membership Committee and Education Committee. He was an Associate Editor of the IEEE TRANSACTIONS ON POWER ELECTRONICS from 2007 to 2012. He is the Transactions Review Chair for the IEEE TRANSACTIONS ON INDUSTRY APPLICATIONS for the Industrial Power Converter Committee.

Fei (Fred) Wang (S'85–M'91–SM'99–F'10) received the B.S. degree from Xi'an Jiaotong University, Xi'an, China, and the M.S. and Ph.D. degrees from the University of Southern California, Los Angeles, CA, USA, in 1982, 1985, and 1990, respectively, all in electrical engineering.

He was a Research Scientist in the Electric Power Lab, University of Southern California, from 1990 to 1992. He joined the GE Power Systems Engineering Department, Schenectady, NY, as an Application Engineer in 1992. From 1994 to 2000, he was a Senior Product Development Engineer with GE Industrial Systems, Salem, VA. During 2000 to 2001, he was the Manager of Electronic & Photonic Systems Technology Lab, GE Global Research Center, Schenectady, NY, and Shanghai, China. In 2001, he joined the Center for Power Electronics Systems (CPES) at Virginia Tech, Blacksburg, VA, as a Research Associate Professor and became an Associate Professor in 2004. From 2003 to 2009, he also served as the CPES Technical Director. Since 2009, he has been with The University of Tennessee and Oak Ridge National Lab, Knoxville, TN, USA, as a Professor and the Condra Chair of Excellence in Power Electronics. He is a founding member and the Technical Director of the multi-university NSF/DOE Engineering Research Center for Ultra-wide-area Resilient Electric Energy Transmission Networks led by The University of Tennessee. His research interests include power electronics, power systems, controls, electric machines and motor drives.

Kevin Tomsovic (F'07) received the B.S. degree in electrical engineering from Michigan Technological University, Houghton, MI, USA, in 1982, and the M.S. and Ph.D. degrees in electrical engineering from the University of Washington, Seattle, WA, USA, in 1984 and 1987, respectively.

He is currently a CTI Professor of the Department of Electrical Engineering and Computer Science at the University of Tennessee, Knoxville, where he also directs the NSF ERC CURENT. Visiting university positions have included Boston University, Boston, MA; National Cheng Kung University, Tainan, R.O.C.; National Sun Yat-Sen University, Kaohsiung, Taiwan, R.O.C.; and the Royal Institute of Technology, Stockholm, Sweden. He was on the faculty of Washington State University from 1992 to 2008.

Dr. Tomsovic held the Advanced Technology for Electrical Energy Chair at Kumamoto University, Kumamoto, Japan, from 1999 to 2000 and was an NSF Program Director in the ECS Division of the Engineering Directorate from 2004 to 2006.